NJC

Accepted Manuscript

This is an *Accepted Manuscript*, which has been through the Royal Society of Chemistry peer review process and has been accepted for publication.

Accepted Manuscripts are published online shortly after acceptance, before technical editing, formatting and proof reading. Using this free service, authors can make their results available to the community, in citable form, before we publish the edited article. We will replace this *Accepted Manuscript* with the edited and formatted *Advance Article* as soon as it is available.

You can find more information about *Accepted Manuscripts* in the Information for Authors.

Please note that technical editing may introduce minor changes to the text and/or graphics, which may alter content. The journal's standard Terms & Conditions and the Ethical guidelines still apply. In no event shall the Royal Society of Chemistry be held responsible for any errors or omissions in this *Accepted Manuscript* or any consequences arising from the use of any information it contains.

ROYAL SOCIETY OF CHEMISTRY

www.rsc.org/njc

Preparation of supported AuPd nanoalloys mediated by ionic liquid-like functionalized SBA-15: structural correlations concerning its catalytic activity

João Paulo Vita Damasceno[a], Camila Marchetti Maroneze[a], Mathias Strauss[b], Fernando Aparecido Sigoli[a], Italo Odone Mazali[a,*]

[a]Functional Materials Laboratory, Department of Inorganic Chemistry, Institute of Chemistry, University of Campinas (UNICAMP), Campinas, São Paulo, Brazil.

[b]Nanostructured Soft Materials Laboratory, Brazilian Nanotechnology National Laboratory (LNNano), National Center for Research in Energy and Materials (CNPEM), Campinas, São Paulo, Brazil.

*Corresponding author

Prof. Dr. Italo Odone Mazali

E-mail address: mazali@iqm.unicamp.br

Abstract

Noble metal nanoalloys are very important in catalysis, sensing, electrochemistry, and plasmonics. Based on the importance of these materials and in order to overcome the synthetic limitations for the synthesis of supported nanoalloys *in situ* in porous supports, we extended a synthetic protocol to achieve supported AuPd nanoalloys within the SBA-15 pores modified with an ionic liquid-like alkoxysilane. The synthesized materials are formed by very small nanoparticles with non-passivated surfaces that are highly active as heterogeneous catalysts for the reduction of 4-nitrophenol. The anion exchange capacity of the functionalized SBA-15 was used to adsorb Au and Pd anionic complexes. The adsorbed species were then reduced and converted into supported monometallic nanoparticles or nanoalloys. Nitrogen physisorption isotherms showed that the entire synthesis process does not damaged the mesoporous support nor blocked the pores. TEM/EDS and UV-vis analysis were used to prove the alloy formation in the bimetallic materials by the concomitant presence of Au and Pd in the same particle and by the gold plasmon band disappearance as the palladium content increased. Finally, the materials catalytic activity increased as the palladium content was enhanced, showing that it is possible to control the catalytic performance by tuning the materials composition during the anion exchange step.

Keywords: SBA-15; Surface functionalization; Ion exchange; Metallic nanoparticles; Nanoalloys; Mesoporous materials; Heterogeneous catalyst; Synthesis *in situ*; Supported nanoparticles; 4-nitrophenol reduction;

1. Introduction

Nanomaterials have gained highlight for the possibility to change their properties in a controlled way, as well as new physical and chemical properties that arises due to the reduced size. Nanoalloys stand out because their properties can be adjusted by changing the atomic array and/or the composition beyond the particles size and morphology [1–3]. However, the achievement of nanoalloys with small sizes is still a big challenge, especially in the *in situ* synthesis of supported alloy nanoparticles.

Noble metal nanoparticles and nanoalloys are very important for heterogeneous catalysis applications. Most of the chemical synthesis of these metal nanoparticles are based on wet methods, like the pioneer work reported by Michael Faraday in 1857 for colloidal gold [4]. These synthesis often use soluble metallic precursors and surface stabilizing agents like polymers, surfactants, dendrimers, or ionic liquids [2,5,6]. Those methods are very efficient to control the particle size, morphology and composition, but they result in colloidal nanoparticles with passivated surface that cannot be separated from the reaction medium. Moreover, the preparation of heterogeneous catalysts from those colloidal particles requires extra steps of immobilization onto a solid support and removing the surface stabilizers before the use of the catalysts.

In order to overcome those synthetic limitations, we propose the use of the mesoporous silica SBA-15 functionalized with an ionic liquid-like alkoxysilane to obtain supported AuPd nanoalloys, with very small sizes (mostly below 5 nm), non-passivated metallic surfaces and tuned compositions. This methodology has been explored for the preparation of supported monometallic nanoparticles, *e.g.* Au NPs supported on functionalized SiO_2 [7], Pd NPs on alumina [8], Au and Pt NPs on carbon nanotubes [9], and Pt NPs on magnetite [10]. We have applied this synthetic approach to obtain *in situ* nanoalloys

supported on the modified SBA-15. The anion exchange capacity of the surface functional groups was used to adsorb noble metal complexes, which were subsequently reduced, resulting in monometallic or alloy nanoparticles. Finally, we evaluated the catalytic performance of the synthetized materials in the reduction of 4-nitrophenol. The correlation between the catalytic activity and particles nanostructuring was studied and showed that the supported nanoparticles are active toward the reaction without removing the ionic liquid from silica surface. Moreover, the catalytic activity can be adjusted by tuning the nanoparticles composition and the increasing in the palladium content was followed by higher values of velocity constants.

2. Experimental Procedure

2.1. Synthesis of mesoporous silica SBA-15

SBA-15 was synthesized according to the procedure described in the literature [11–13]. In a typical synthesis, 5.0 g of Pluronic P-123 was dissolved in 187.5 mL of 1.6 mol L^{-1} HCl aqueous solution under vigorous stirring (mechanical paddle stirrer, 70-130 W, 1000 rpm) at 313 K in a water bath. The system was stirred for 2 h before the addition of 11.38 mL of TEOS (tetraethyl orthosilicate). The solution was kept under stirring for 8 min and then under static conditions at 313 K for 24 h. The mixture was then transferred to autoclaves (polytetrafluoroethylene vessels) and treated at 373 K for 24 h. The solid product was washed with deionized water and ethanol, dried at 373 K overnight, and thermally treated at 823 K for 6 h (2 °C min^{-1}) under air flow to eliminate the organic template from the pores. The sample was named as SBA-15.

2.2. Synthesis of 1-methyl-3-[(3- trimethoxysilane)-n-propyl]-imidazolium chloride (Imi^+)

The ionic liquid-based alkoxysilane was synthetized according to a procedure described in the literature [7,8,14]. In a round-bottom flask with 13.1 mL of dry toluene, 9.12 mL of (3-chloropropyl)trimethoxysilane and 3.99 mL of 1-methylimidazole were added simultaneously. The mixture was maintained under stirring at 368 K during 24 h. After that, the system was kept under static conditions until the complete phase separation, being the bottom phase the desired alkoxysilane.

2.3. SBA-15 surface functionalization with Imi^+ entities

1 g of SBA-15 was suspended in a solution containing 100 mL of dry ethanol and 0.542 mL (20 mmol L^{-1}) of the as-prepared alkoxysilane. The mixture was kept under reflux for 24 h under vigorous stirring. After this period, the functionalized silica was washed twice with 100 mL of ethanol to remove most of the non-covalent attached molecules, and dried at 373 K overnight. The material was named as SBA-15-Imi^+.

2.4. Synthesis of supported metal nanoparticles

200 mg of SBA-15-Imi^+ was immersed in 25 mL of aqueous solution of $HAuCl_4 \cdot 3H_2O$ and K_2PdCl_4, individually or in mixtures, with total noble metal concentration of 1 mmol L^{-1}. The suspension was stirred for 2 h at ambient temperature to promote the ion exchange between chloride and metal complexes anions. Then, it was washed four times with 50 mL of deionized water and dried at 373 K overnight. The concentration of each metal precursor varied from 0.1 to 1.0 mmol L^{-1}.

The solids containing the adsorbed metal complexes were immersed in 25 mL of $NaBH_4$ aqueous solution (10 mmol L^{-1}) for 30 min. The materials were washed with 50 mL of deionized water, 50 mL of HCl aqueous solution (0.1 mol L^{-1}) and three more times with 50 mL of deionized water respectively, and then dried at 373 K overnight. The samples were named as SBA-15-Imi^+ followed by the metal ratios used in the synthesis, for example SBA-15-Imi^+-Au0.90Pd0.10 (see Table 1).

2.5. Adsorption isotherms for metallic complexes on SBA-15-Imi^+ material

25 mg of SBA-15-Imi^+ was immersed in 10 mL of aqueous solution of $HAuCl_4 \cdot 3H_2O$ or K_2PdCl_4 with concentrations between 0.05 to 1.40 mmol L^{-1}. The contact was maintained at 298 K for 2 h. Then, the solids were isolated and the amount of Au or Pd in the supernatant solutions was quantified by ICP-OES to determine the equilibrium concentration ($C_{eq.}$) [15,16].

2.6. Catalytic tests for the 4-nitrophenol reduction

The molar ratio of 1:10:500 for supported metal, 4-nitrophenol (4-NP) and sodium borohydride was used for all tests. Suspensions of the catalysts in water (20 mg mL^{-1}) were sonicated for 15 min (40 kHz) before the catalytic tests.

The reactions were conducted in a quartz cuvette, at 298 K and magnetic stirring, and total volume equal to 3 mL. The reaction progress was monitored by acquiring UV-vis spectrum in intervals of one second during 10 min. Scattering effects of the suspended silica particles were discounted by blank measurements of the respective catalyst dispersions in water.

2.7. Samples characterization

Solid-state cross-polarization magic angle spinning nuclear magnetic resonance spectra (CP/MAS NMR) of ^{13}C and ^{29}Si were obtained on a Bruker 400 spectrometer, with the chemical shifts calibrated against the tetramethylsilane (TMS) standard.

The quantity of organic groups bonded to the silica surface was estimated from the nitrogen content, which was determined by means of elemental analyses on a Perkin-Elmer 2400 equipment.

Quantification of metals was made with ICP-OES using a Perkin-Elmer Optima 8300 equipment. The samples were prepared by adding about 20 mg of each catalyst at 15 mL polypropylene tubes, followed by 1 mL of HF 48 %, aqua regia enough to make a clear solution (between 1 and 2 mL), and water until 15 mL.

The N_2 adsorption-desorption isotherms were measured at 77 K in a Micromeritics equipment, model ASAP 2020. The samples were previously outgassed under vacuum during 12 h at 303 K before analysis to achieve pressure value less than 10 μmHg. The BET (Brunauer-Emmett-Teller) and BJH (Barrett-Joyner-Halenda) methods were used for the determination of specific surface area and average pores diameters respectively.

Diffuse reflectance spectroscopy was done on an ultraviolet-visible-near-infrared (UV-vis-NIR) Cary 5000 spectrometer equipped with an integrating sphere spectral collector. The spectra were acquired in the 200-800 nm range and $BaSO_4$ powder was used for the instrumental background correction.

Transmission Electron Microscopy (TEM) images and Energy Dispersive X-ray Spectroscopy (TEM-EDS) analysis were performed at the Brazilian Nanotechnology National Laboratory (LNNano). TEM analyzes were done using a JEOL JEM 2100 microscope, with acceleration voltage of 200 kV and LaB_6 thermionic filament as electron

source. TEM-EDS analysis was performed utilizing a JEOL JEM 2100F microscope, operating with acceleration voltage of 300 kV, with a field emission electron gun (FEG). The samples for electronic microscopy were suspended in water and kept in ultrasonic bath for 30 min, and then the suspensions were deposited in copper grids covered with carbon film (200 mesh).

The catalytic experiments were performed on an Agilent UV-vis spectrometer, model 8453, coupled to a Peltier HP89090A, and the spectra were recorded between 200 and 800 nm.

3. Results and Discussions

The general procedure carried out for the *in situ* synthesis of the supported mono- or bimetallic nanoparticles composed of Au and/or Pd is illustrated in Figure 1.

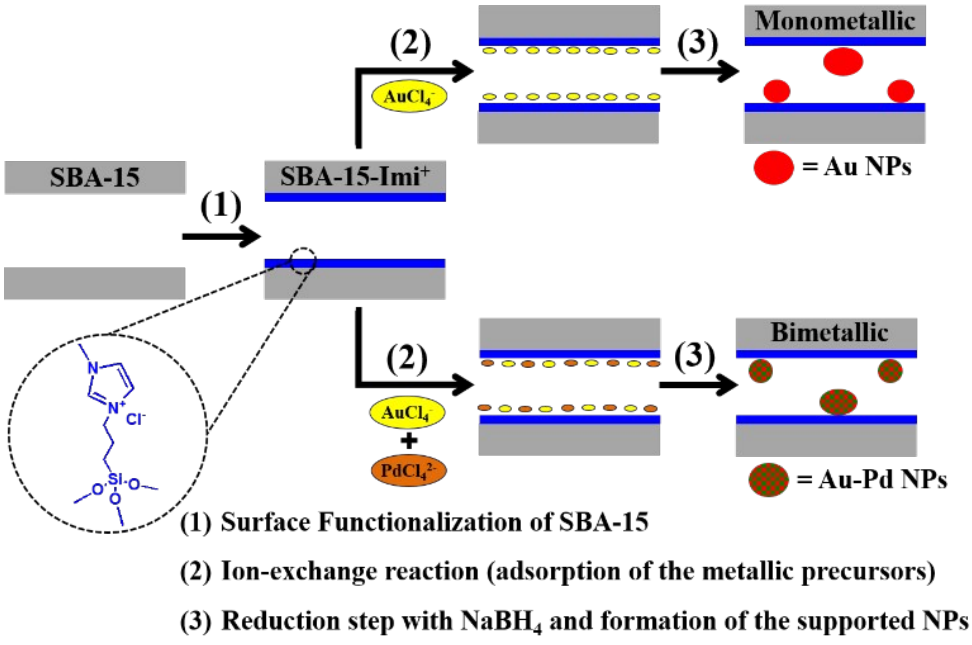

Figure 1. Schematic illustration of the procedure carried out for the *in situ* synthesis of the supported mono- and bimetallic nanoparticles.

The first step (1) consisted in the surface functionalization of the SBA-15 support according to the procedure described elsewhere [7,8]. The confirmation that the imidazolium moieties were chemically bonded to the silica surface was done by ^{13}C and ^{29}Si CP/MAS NMR of the SBA-15 and SBA-15-Imi^+ materials (Figures S1 and S2 in the Supporting Information (SI)). All the observed peaks were properly attributed and are in agreement with previously reported literature [7,8,14]. The amount of the organic functional groups in the SBA-15-Imi^+ sample determined by elemental analysis was 0.5 mmol per gram. The calculus was based on the N content (1.4 wt%).

The second step (2) makes use of the anion-exchange properties of the imidazolium groups [7,17] attached to the surface to uptake the metallic precursors (complex anions) into the porous structure, which are kept strongly adsorbed on the functionalized surface by electrostatic interactions, and that are subsequently converted into supported metallic particles by chemical reduction with $NaBH_4$ (step (3)).

The adsorption/ion-exchange isotherms for $AuCl_4^-$ and $PdCl_4^{2-}$ on the SBA-15-Imi^+ are shown in Figure 2.

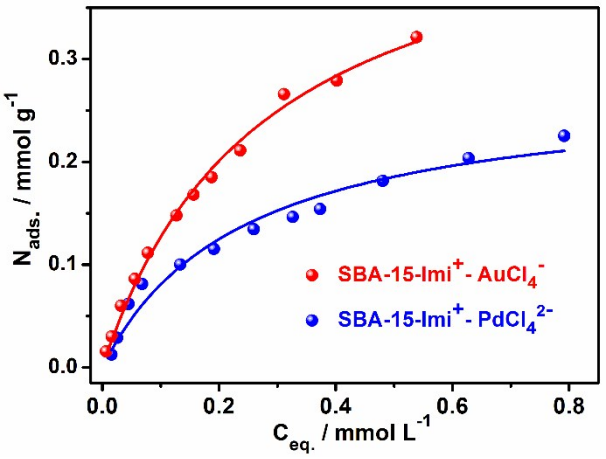

Figure 2. Adsorption isotherms for the anionic complexes $AuCl_4^-$ and $PdCl_4^{2-}$ on the SBA-15-Imi^+ sample at 298 K and the respective Langmuir fits.

As expected, the ion-exchange stoichiometry, which is 1:1 for Imi^+:$AuCl_4^-$ and 2:1 for Imi^+:$PdCl_4^{2-}$, play a pivotal role for the higher effective ion-exchange capacity of the $AuCl_4^-$ precursor when compared to $PdCl_4^{2-}$, which are respectively 0.48 and 0.27 mmol g^{-1}. Table 1 summarizes the metal content (wt%) for the samples with variable Au/Pd compositions (after the reduction step).

Table 1. Au and Pd wt% in the synthesized samples with variable Au/Pd content and the respective nominal and experimental molar compositions.

Material	Au wt%	Pd wt%	Metal content / 10^{-2} mmol g^{-1}	Exp. Comp.
SBA-15-Imi^+-Au1.00	1.74	-	8.8	Au1.00
SBA-15-Imi^+-Au0.90Pd0.10	1.67	0.07	9.2	Au0.93Pd0.07
SBA-15-Imi^+-Au0.75Pd0.25	1.39	0.19	8.8	Au0.80Pd0.20
SBA-15-Imi^+-Au0.50Pd0.50	0.85	0.30	7.1	Au0.61Pd0.39
SBA-15-Imi^+-Au0.25Pd0.75	0.40	0.33	5.2	Au0.39Pd0.61
SBA-15-Imi^+-Au0.10Pd0.90	0.16	0.30	3.6	Au0.22Pd0.78
SBA-15-Imi^+-Pd1.00	-	0.32	3.0	Pd1.00

As discussed before, when comparing the materials SBA-15-Imi^+-Au1.00 and SBA-15-Imi^+-Pd1.00, it is noted that the sample containing only Au has approximately 3 times more metal (molar amount) than the Pd one. It was also observed that for all the materials containing both metals, there is always the same trend concerning the enrichment of Au content on the final composition of the samples when compared to the initial nominal values used in the ion-exchange reaction.

The porosity of the SBA-15, SBA-15-Imi$^+$, SBA-15-Imi$^+$-Au1.00 and SBA-15-Imi$^+$-Pd1.00 materials was evaluated by nitrogen physisorption isotherms (Figure 3).

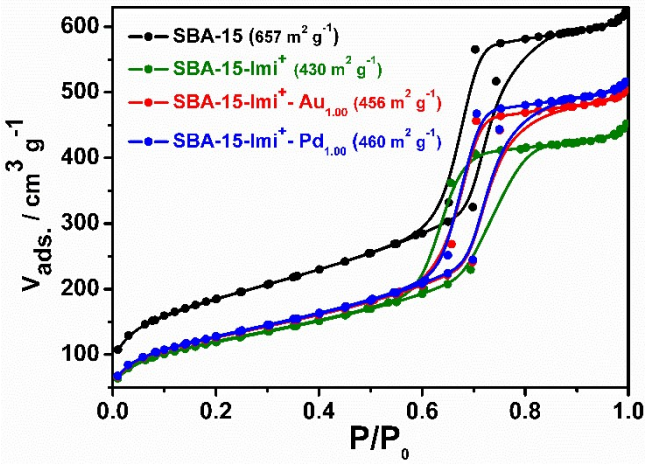

Figure 3. Nitrogen physisorption isotherms for SBA-15, SBA-15-Imi$^+$, SBA-15-Imi$^+$-Au1.00 and SBA-15-Imi$^+$-Pd1.00 samples.

All curves are type IV isotherms, characteristic of mesoporous materials. The hysteresis are typical of porous materials formed by well-defined cylindrical-like pore channels and uniform pores size (type H1), such as SBA-15 materials [11,18]. The isotherms for the functionalized and metal-containing samples exhibit hysteresis loops with less uniformity (less parallel branches) compared to the SBA-15 reference material. This lower symmetry together with the decrease of the specific surface area values are consistent with the surface modification processes [19], and shows that the imidazolium groups are distributed mainly along the pores surface. No obstruction or blocking of the pores were observed after the surface functionalization and after the formation of the supported metallic particles, based on the one-step desorption, evidencing that the entire process does not affect the accessibility to the metallic sites into the porous structure, which is an extremely important feature for catalytic purposes.

TEM images for the SBA-15-Imi$^+$-Au1.00 and SBA-15-Imi$^+$-Pd1.00 samples are shown in Figure 4, and corroborate with the N_2 physisorption results discussed above.

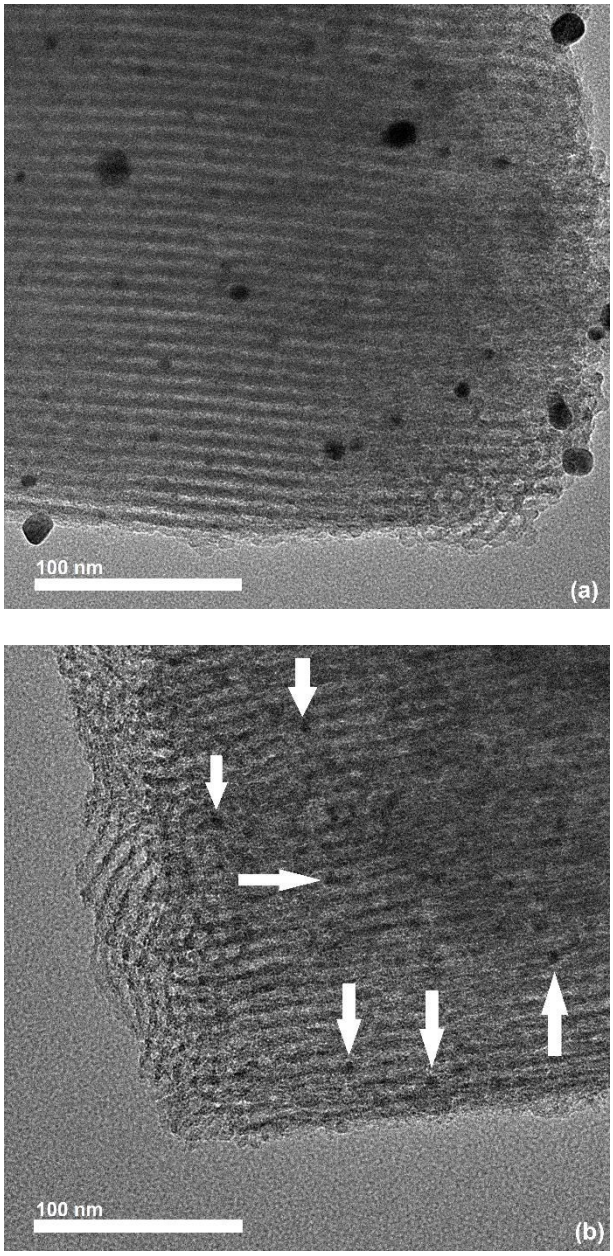

Figure 4. TEM images of SBA-15-Imi$^+$-Au1.00 in (a) and SBA-15-Imi$^+$-Pd1.00 in (b).

The electron micrographs from Figure 4 reveal the regular porous structure of SBA-15 and confirm that the metallic structures are present as nanoparticles, well dispersed into the pores and sparsely located on the outer surface (only in the case of the

SBA-15-Imi^{+}-Au1.00 sample). The images also show that the higher metal content for the SBA-15-Imi^{+}-Au1.00 results in bigger particles when compared to the SBA-15-Imi^{+}-Pd1.00 material, which seems to be only composed by very small nanostructures distributed all over the pores. The ionic liquid-like alkoxysilane attached to the silica surface along with the silica pore structure are responsible for the nanoparticles stabilization, which dispenses the use of other stabilizing agent to control the size of the nanostructures as discussed previously [7] and avoids the leaching of nanoparticles during the catalytic tests.

The synthetic procedure resulted in very small metallic nanoparticles with diameters mostly smaller than 5 nm. Such feature is important for metal saving and appears to have influence over the selectivity of noble metal heterogeneous catalysts according the works of the Somorjai research group [2,20].

The presence of both metals on the Au-Pd samples do not guarantee the obtainment of alloy nanoparticles, since the metals can form core-shell, segregated monometallics or alloy nanoparticles. The confirmation that the adopted synthesis procedure resulted in the formation of nanoalloys was achieved by TEM-EDS and DRS measurements that are shown in Figure 5.

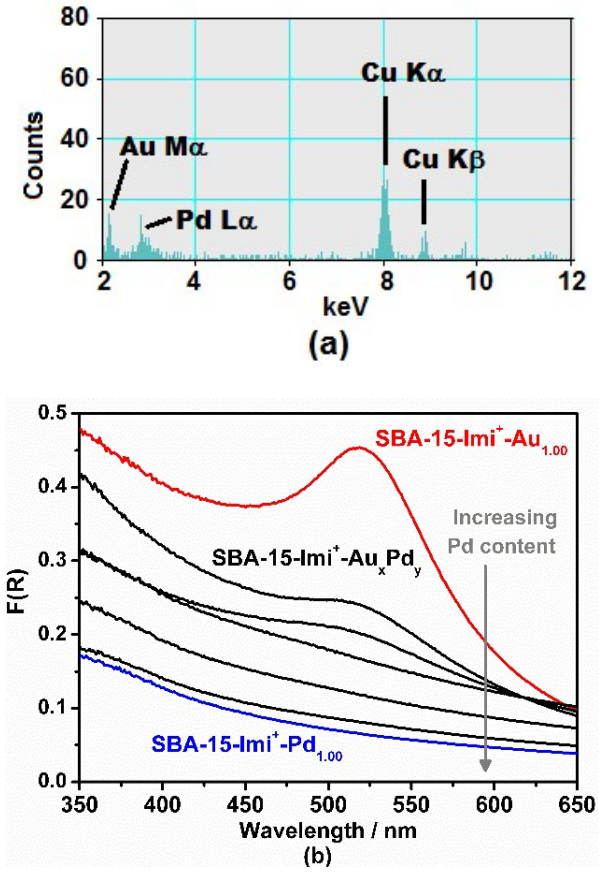

Figure 5. (a) TEM-EDS spectrum for the SBA-15-Imi^{+}-Au0.25Pd0.75 sample, and signals from Cu are referent from sample holder; (b) The DRS spectra of the synthesized materials; Colored spectra are referent to SBA-15-Imi^{+}-Au1.00 and SBA-15-Imi^{+}-Pd1.00 samples respectively.

Figure 5 (a) shows the TEM-EDS spectrum of a single particle analyzed from the SBA-15-Imi^{+}-Au0.25Pd0.75 sample (the respective TEM image is shown in Figure S3 (SI)). The signals with energies equal to 2.1 and 2.9 eV are referent to Au and Pd respectively [21]. The spectrum shows that both metals are distributed along the analyzed area, which is nearly the size of a single particle. The Au and Pd signals present relative small intensities because of the low metal content, as well as because the EDS spectrum is referent to a single particle. However, the punctual analysis was important to give local information about the composition, but is not enough to conclude if both metals are present at the particle as alloy or segregated phases.

The confirmation of the alloy formation was given by the DRS measurements presented in Figure 5 (b). The spectrum of the SBA-15-Imi^{+}-Au1.00 material shows the surface plasmon band centered at 519 nm, characteristic for gold-based nanostructures with spherical shape [22]. The region between 200 and 350 nm (not shown) exhibited an adsorption band centered at 215 nm related to the electronic transition of the 1-methylimidazolium ring.

The increasing in the palladium content in the materials was accompanied by the spectral changes expected for alloy nanoparticles. According to the literature [23–27], Au-Pd alloy formation is indicated by the shift of the X-ray diffraction peaks of gold to higher 2θ angles as well as by the disappearance of the gold plasmon band as the palladium content increases. At the same time, this content increases is accompanied by the appearance of a band that begins at the visible region and grows exponentially in the ultraviolet region, which is typical for metallic palladium nanoparticles [28]. Such behavior is observed in the DRS spectra (Figure 5 (b)) for the synthetized bimetallic nanostructures studied in this work and confirms the formation of AuPd nanoalloys.

The catalytic properties of the synthesized materials were then evaluated towards the reduction reaction of 4-nitrophenol (4-NP). The reaction of 4-NP with sodium borohydride in aqueous medium is a probe reaction for metallic nanoparticles catalytic activity. There is an extensive database concerning this reaction catalyzed by different metallic nanosystems [29–32], and even by transition metal oxides [33]. The reaction is thermodynamically favorable as the electrochemical semi-potentials reveal [34,35], but the activation barrier is high enough to the reaction do not proceed in appreciable timescales at ambient conditions without a catalyst. This condition, along with no side reactions, full kinetic analysis of the reaction at different temperatures, mild reactional conditions of

temperature and pressure and the use of mild solvents like water, make this a model reaction to metallic nanoparticles characterization [29]. UV-Vis spectroscopy is commonly used to monitor the concentrations of the reactant and product since 4-NP exhibits an absorption band with maximum at 377 nm, and the product 4-aminophenol (4-AP) has a band centered at 290 nm approximately [29,36].

The velocity constant is commonly obtained from the values of absorbance at 400 nm against time, because the band relative to 4-NP has its maximum shifted to 400 nm due to the formation of 4-nitrophenolate ion in the reaction conditions [29,36]. During the reaction, the absorption band at 400 nm shows exponential decrease along time. Even being dependent on the concentrations of 4-NP and $NaBH_4$, the reduction can be considered a pseudo-first-order reaction in respect to 4-NP when it is carried out with excess of $NaBH_4$ [37]. This assumption was considered for the kinetic analysis in this work.

Figure S4 (SI) exhibits the absorbance versus the wavelength for the reaction catalyzed by SBA-15-Imi$^+$-Au0.75Pd0.25 material, showing the typical spectral change over the time for this reaction. Absorbance decrease in the 4-nitrophenolate band and the increase in the 4-AP band indicate the progress of the reduction reaction, with no byproducts formation [29,31], by the isosbestic point around 323 nm. Figure S5 (SI) shows the absorbance at 400 nm versus the time for the control catalytic tests: without solid, with SBA-15, and SBA-15-Imi$^+$ materials. No decrease in the absorbance intensity at 400 nm was observed at all these tests (as well as no increase in intensity at 300 nm), indicating that 4-NP was not reduced in the absence of the metallic nanoparticles.

The absorbance at 400 nm versus time and the apparent velocity constants for 4-NP reduction reactions carried out with the seven synthetized materials are presented in Figure 6. The respective constants values are shown in Table S1 (SI).

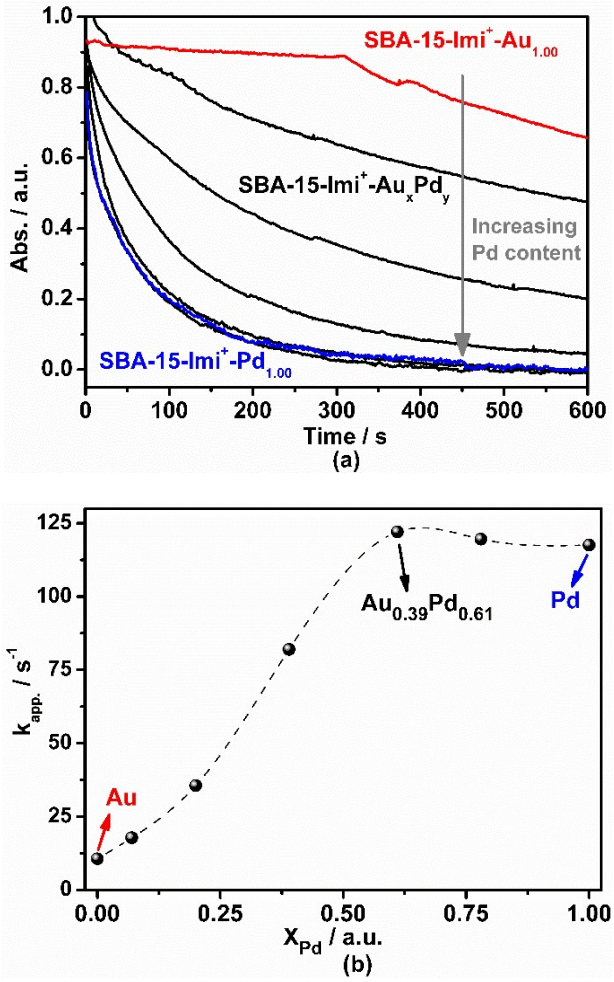

Figure 6. (a) Absorbance at 400 nm versus time for 4-NP reduction catalyzed with the synthesized materials; (b) Apparent velocity constants for 4-NP reduction versus molar fraction of Pd on the synthetized materials.

The kinetics studies that have been reported in the literature indicate that 4-NP reduction with $NaBH_4$ aqueous solution proceeds via Langmuir-Hinshelwood mechanism and it is assumed that both reagents must be chemisorbed on the catalyst to the reaction proceeds [37]. After the adsorption of the borohydride ions, some catalysts undergo a surface restructuring before the reaction starts, which is called the induction period [37,38]. Only the SBA-15-Imi$^+$-Au1.00 sample exhibited the induction period, as shown in Figure 6 (a), with no significant decrease in the absorbance until 310 seconds.

The SBA-15-Imi$^+$-Au1.00 sample exhibited the lowest apparent velocity constant, but there are many examples of gold nanoparticles as very active catalysts for the 4-NP reduction [30,31]. The reported values for apparent velocity constants are very diversified and are mainly dependent on the particles sizes, morphologies and stabilizing agents attached to the metallic surface. Regarding the synthetized materials, SBA-15-Imi$^+$-Au1.00 has some big nanoparticles outside the SBA-15 pores, but the majority are small particles located inside the pores. Then, the low catalytic activity of the Au catalyst toward the 4-nitrophenol reduction seems to be consequence of the nanoparticles nanostructuring as well as the contact with the imidazolium groups.

The apparent velocity constant values obtained for the catalyzed reduction reaction with the synthetized materials are in agreement with the values reported in the literature for highly active systems [30–32,39–43]. This high activity together with the absence of the inductive period make the palladium-rich materials very attractive for reduction of nitroaromatic compounds.

Besides, most of the stabilizers must be removed from the surface of the metallic nanoparticles before catalytic reactions to make the active sites available. However, the catalytic activity toward the 4-nitrophenol reduction using the SBA-15-Imi$^+$-metal catalysts showed that it is not necessary to remove the ionic liquid-like alkoxysilane from silica to have active particles.

The velocity constants values increase with higher palladium content, so that the catalysts reactivity is tuned by the composition of supported nanoalloys. The changes in the velocity constants values are due to the achievement of new surface and electronic structures in those nanoalloys. Such nanostructures may have “magic” compositions with higher reactivity and/or stability, in addition to the traditional “magic” sizes shown by

monometallic clusters or nanoparticles [3]. The data from Figure 6 show that the nanoalloys with high palladium content do not have catalytic activity very distinct from the SBA-15-Imi^{+}-Pd1.00 sample, which indicates that the activity of the palladium fraction in these alloy particles dominates its catalytic constant values, so that the changes in electronic and surface structures of the synthetized nanoalloys are not enough to cause significant for the catalytic activity against 4-NP reduction.

4. Conclusion

SBA-15 modification with the cationic ionic liquid-like alkoxysilane moieties provided anion-exchange properties to the mesoporous solid, which allowed the adsorption of anionic noble metal complexes. These metallic entities were reduced and converted into supported monometallic (Au or Pd) nanoparticles or AuPd nanoalloys.

The adsorption behavior of the metallic complexes was studied and tuned the nanoalloys final compositions. The mesoporous structure of the SBA-15 was not altered by the functionalization nor by the reduction procedure. The resulting supported nanoparticles are very small (between 1 and 5 nm), have non passivate surfaces, and are highly dispersed throughout the silica. The nanoalloy formation was confirmed by EDS analysis, which showed the presence of Au and Pd in the same particle, combined with DRS measurements that revealed the gold plasmon band disappearance as palladium content increased.

The materials catalytic activity was tested towards the 4-nitrophenol reduction. The velocity constants increased as a function of the palladium content.

5. Acknowledgment

JPVD would like to thank the São Paulo Research Foundation (FAPESP) for scholarship (process 2013/24400-8). CMM would like to thank the National Council for Scientific and Technological Development (CNPq). The authors thank also the Brazilian Nanotechnology National Laboratory (LNNano) at Campinas for the Transmission Electron Microscopy analysis and the Solid State Chemistry Laboratory (LQES) at University of Campinas for the nitrogen physisorption analysis.

6. References

1 K. An and G. A. Somorjai, *Catal. Letters*, 2015, **145**, 233–248.

2 G. A. Somorjai and J. Y. Park, *Angew. Chemie Int. Ed.*, 2008, **47**, 9212–9228.

3 R. Ferrando, J. Jellinek and R. L. Johnston, *Chem. Rev.*, 2008, **108**, 845–910.

4 M. Faraday, *Philos. Trans. R. Soc. London*, 1857, **147**, 145–181.

5 H. Hu, J. H. Xin, H. Hu, X. Wang, D. Miao and Y. Liu, *J. Mater. Chem. A*, 2015, **3**, 11157–11182.

6 X. Liu, D. Wang and Y. Li, *Nano Today*, 2012, **7**, 448–466.

7 N. Fattori, C. M. Maroneze, L. P. da Costa, M. Strauss, F. A. Sigoli, I. O. Mazali and Y. Gushikem, *Langmuir*, 2012, **28**, 10281–10288.

8 L. Luza, A. Gual, D. Eberhardt, S. R. Teixeira, S. S. X. Chiaro and J. Dupont, *ChemCatChem*, 2013, **5**, 2471–2478.

9 H. Zhang and H. Cui, *Langmuir*, 2009, **25**, 2604–2612.

10 R. Abu-Reziq, D. Wang, M. Post and H. Alper, *Adv. Synth. Catal.*, 2007, **349**, 2145–2150.

11 D. Zhao, J. Feng, Q. Huo, N. Melosh, G. H. Fredrickson, B. F. Chmelka and G.

D. Stucky, *Science*, 1998, **279**, 548–552.

12 D. Zhao, Q. Huo, J. Feng, B. F. Chmelka and G. D. Stucky, *J. Am. Chem. Soc.*, 1998, **120**, 6024–6036.

13 V. Meynen, P. Cool and E. F. Vansant, *Microporous Mesoporous Mater.*, 2009, **125**, 170–223.

14 P. Han, H. Zhang, X. Qiu, X. Ji and L. Gao, *J. Mol. Catal. A Chem.*, 2008, **295**, 57–67.

15 A. W. Adamson and A. P. Gast, *Physical Chemistry of Surfaces*, John Wiley & Sons, 6ª ed, 1997.

16 F. Rouquerol, J. Rouquerol and K. Sing, *Adsorption by Powders and Porous Solids: Principles, Methodology and Applications*, Academic Press, 1999.

17 N. Fattori, C. M. Maroneze, L. P. Da Costa, M. Strauss, I. O. Mazali and Y. Gushikem, *Colloids Surfaces A Physicochem. Eng. Asp.*, 2013, **437**, 120–126.

18 N. N. Greenwood, A. Earnshaw, Chemistry of the Elements, Elsevier, 2ª ed., 1997.

19 C. M. Maroneze, H. A. Magosso, A. V. Panteleimonov, Y. V. Kholin and Y. Gushikem, *J. Colloid Interface Sci.*, 2011, **356**, 248–256.

20 K. An and G. A. Somorjai, *ChemCatChem*, 2012, **4**, 1512–1524.

21 T. A. G. Silva, E. Teixeira-Neto, N. López and L. M. Rossi, *Sci. Rep.*, 2014, **4 : 5766**, 1–5.

22 A. Moores and F. Goettmann, *New J. Chem.*, 2006, **30**, 1121–1132.

23 C. Kan, W. Cai, C. Li, L. Zhang and H. Hofmeister, *J. Phys. D. Appl. Phys.*, 2003, **36**, 1609–1614.

24 F. Liu, D. Wechsler and P. Zhang, *Chem. Phys. Lett.*, 2008, **461**, 254–259.

25 M. O. Nutt, J. B. Hughes and M. S. Wong, *Environ. Sci. Technol.*, 2005, **39**, 1346–

1353.

26 C.-H. Liu, R.-H. Liu, Q.-J. Sun, J.-B. Chang, X. Gao, Y. Liu, S.-T. Lee, Z.-H. Kang and S.-D. Wang, *Nanoscale*, 2015, **7**, 6356–6362.

27 S. Kunz and E. Iglesia, *J. Phys. Chem. C*, 2014, **118**, 7468–7479.

28 S. Sarina, H.-Y. Zhu, Q. Xiao, E. Jaatinen, J. Jia, Y. Huang, Z. Zheng and H. Wu, *Angew. Chemie Int. Ed.*, 2014, **53**, 2935–2940.

29 P. Hervés, M. Pérez-Lorenzo, L. M. Liz-Marzán, J. Dzubiella, Y. Lu and M. Ballauff, *Chem. Soc. Rev.*, 2012, **41**, 5577–5587.

30 C. Deraedt, L. Salmon, S. Gatard, R. Ciganda, R. Hernandez, J. Ruiz and D. Astruc, *Chem. Commun.*, 2014, **50**, 14194–14196.

31 T. Aditya, A. Pal and T. Pal, *Chem. Commun.*, 2015, **51**, 9410–9431.

32 J.-H. Noh and R. Meijboom, *Appl. Surf. Sci.*, 2014, **320**, 400–413.

33 T. R. Mandlimath and B. Gopal, *J. Mol. Catal. A Chem.*, 2011, **350**, 9–15.

34 S. Saha, A. Pal, S. Kundu, S. Basu and T. Pal, *Langmuir*, 2010, **26**, 2885–2893.

35 A. Gangula, R. Podila, R. M, L. Karanam, C. Janardhana and A. M. Rao, *Langmuir*, 2011, **27**, 15268–15274.

36 N. Pradhan, A. Pal and T. Pal, *Langmuir*, 2001, **17**, 1800–1802.

37 S. Gu, S. Wunder, Y. Lu, M. Ballauff, R. Fenger, K. Rademann, B. Jaquet and A. Zaccone, *J. Phys. Chem. C*, 2014, **118**, 18618–18625.

38 S. Wunder, Y. Lu, M. Albrecht and M. Ballauff, *ACS Catal.*, 2011, **1**, 908–916.

39 C. Wang, F. Yang, W. Yang, L. Ren, Y. Zhang, X. Jia, L. Zhang and Y. Li, *RSC Adv.*, 2015, **5**, 27526–27532.

40 S. M. El-Sheikh, A. A. Ismail and J. F. Al-Sharab, *New J. Chem.*, 2013, **37**, 2399–2407.

41 J. Zhang, G. Chen, D. Guay, M. Chaker and D. Ma, *Nanoscale*, 2014, **6**, 2125–2130.

42 A. Ma, J. Xu, X. Zhang, B. Zhang, D. Wang and H. Xu, *Sci. Rep.*, 2014, **4**, 4849.

43 B. Naik, S. Hazra, V. S. Prasad and N. N. Ghosh, *Catal. Commun.*, 2011, **12**, 1104–1108.

Table of Contents

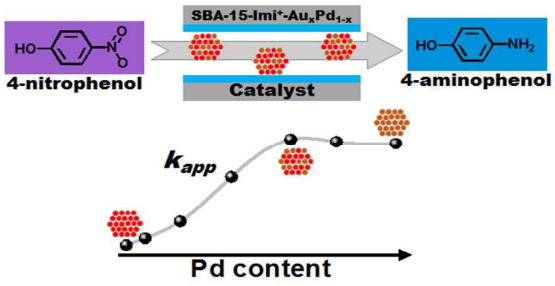

Highly active catalysts based on mono or bimetallic Au and Pd nanoparticles supported in ionic-liquid like modified SBA-15.